

PLATO Hand: Shaping Contact Behavior with Fingernails for Precise Manipulation

Dong Ho Kang¹, Aaron Kim¹, Mingyo Seo¹, Kazuto Yokoyama², Tetsuya Narita², and Luis Sentis¹

Abstract—We present the PLATO Hand, a dexterous robotic hand with a hybrid fingertip that embeds a rigid fingernail within a compliant pulp. This design shapes contact behavior to enable diverse interaction modes across a range of object geometries. We develop a strain-energy-based bending-indentation model to guide the fingertip design and to explain how guided contact preserves local indentation while suppressing global bending. Experimental results show that the proposed robotic hand design demonstrates improved pinching stability, enhanced force observability, and successful execution of edge-sensitive manipulation tasks, including paper singulation, card picking, and orange peeling. Together, these results show that coupling structured contact geometry with a force-motion transparent mechanism provides a principled, physically embodied approach to precise manipulation. Our project page is at: <https://platohand.github.io/plato>.

Index Terms—Multifingered Hands, Mechanism Design, Dexterous Manipulation

I. INTRODUCTION

HUMAN-LIKE dexterity in robotic hands requires both kinematic versatility and effective force regulation at the contact interface. Early work focused on achieving diverse grasp postures and expanded reachable workspace within constrained form factors [1–5]. To accomplish this, designers employed complex mechanisms including tendon-driven transmissions [6–11], spatial linkages [12, 13], and serially stacked servo motors [14–16]. While these approaches successfully expanded kinematic capability, they introduced a critical limitation: high mechanical impedance in the force transmission path. This degrades force-motion transparency and makes compliant, force-regulated interactions difficult to achieve [17–19].

Effective dexterous manipulation depends critically on how contact forces are established and modulated at the fingertip itself [20, 21]. In human fingertips, the mechanical coupling between the nail and underlying soft tissue governs these interactions by constraining local deformation and shaping force transmission pathways [22]. The nail increases local stiffness, limits soft-tissue deformation, and concentrates contact pressure, enabling precise force application at fine spatial scales. Human studies show that subjects with approximately 2 mm fingernails demonstrate significantly enhanced manipulation dexterity [23]. Despite this influence on fingertip mechanics, artificial nails in robotic hands have received limited functional investigation. Prior designs [24–28] employ nails primarily as grasp aids rather than examining how they reshape stiffness distribution, deformation pathways, or force transmission. As

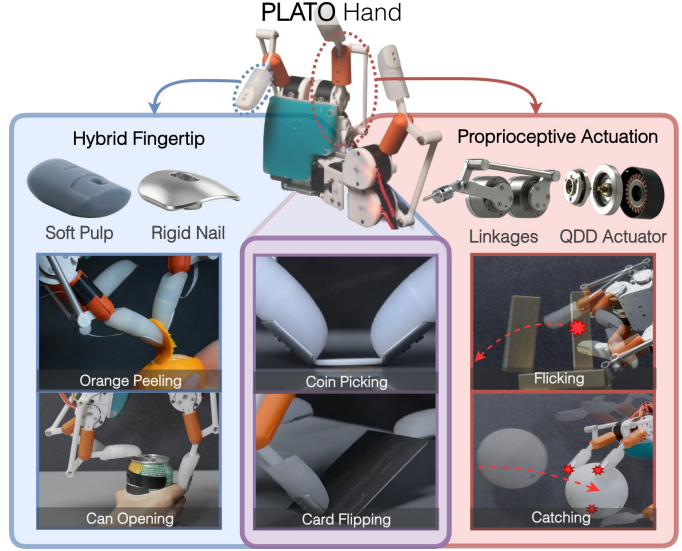


Fig. 1: Overview of the PLATO Hand. This system combines a hybrid fingertip with a rigid fingernail and a compliant fingerpulp to structure local contact mechanics, together with proprioceptive actuation for high-bandwidth force-regulated interactions. This integration enables robust and responsive contact behaviors across a range of precise, dexterous manipulation tasks

fine manipulation tasks become more demanding, robotic hand design must move beyond morphological mimicry toward functional principles that govern human fingertips, including how nails structure contact geometry and enable force-regulated interaction.

To address these limitations, we present the PLATO (Proprioceptive Linkage-driven Anthropomorphic) Hand, which introduces a hybrid contact mechanism that pairs a rigid fingernail with a compliant fingerpulp. The fingernail increases flexural rigidity at the fingertip, which stabilizes the soft fingerpulp. This increases contact surface area and enables adaptive, stable grasping. The fingernail also provides concentrated, rigid contact for transparent force transmission. When combined with proprioceptive actuation [17], this enables high-fidelity force interaction. By fluidly transitioning between precise force control and stable contact, the PLATO Hand achieves fine manipulation capability across diverse contact-rich tasks.

In this paper, we introduce an energy-based model that captures deformation partitioning between global bending and local contact indentation in a hybrid fingernail–pulp fingertip. The model reveals curvature- and material-dependent deformation behavior that shapes contact stability. Based on this model, we design a fingertip and five-bar transmission mechanism that achieves consistent force transmission across the workspace, enabling reliable proprioceptive force sensing. Experiments show that the hybrid fingertip improves pinching stability by

¹ D.H. Kang, A. Kim, M. Seo, and L. Sentis are with The University of Texas at Austin, Austin, TX, USA dongho@utexas.edu

² K. Yokoyama and T. Narita are with the Sony Group Corporation, Toyoko, Japan

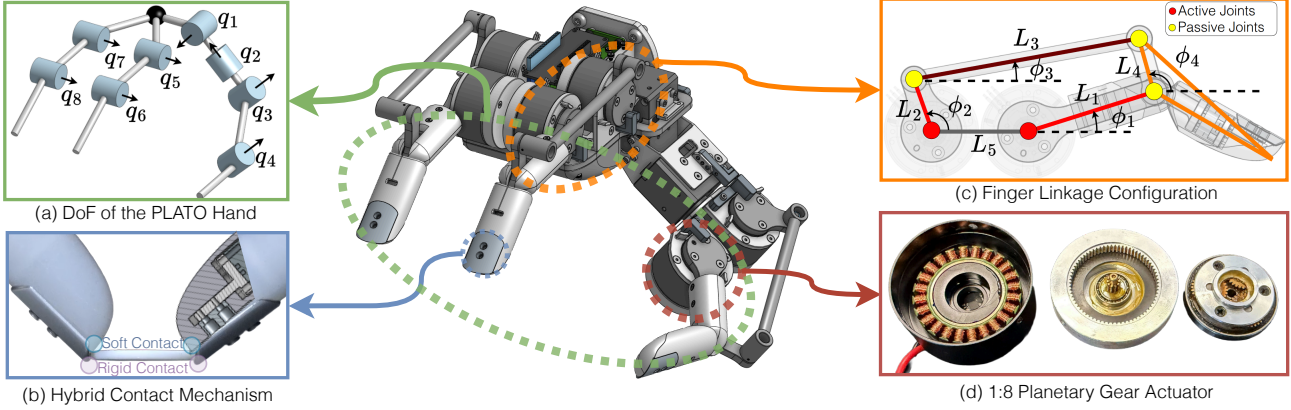


Fig. 2: Design overview of the PLATO Hand. (a) Robot kinematic diagram of the hand with eight fully actuated joints across three fingers: two-DoF index and middle fingers, and a four-DoF thumb. (b) Cross-sectional view of the hybrid fingertip showing a rigid fingernail integrated with a compliant pulp surrounding the distal phalanx and a distal force-torque sensor. (c) Five-bar linkage mechanism coupling the QDD actuators to the finger joints, enabling low-inertia transmission and configuration-dependent torque amplification. (d) Internal structure of the 1:8 ratio planetary gearbox and Outrunner BLDC motor.

23–78% across planar and curved surfaces, enables over 80% success in thin-object manipulation only when the fingernail is present, and increases force-sensing sensitivity by approximately 8 dB at low frequencies and over 20 dB at high frequencies. The core contributions of this work are:

- i) An energy-based fingertip model showing how material stiffness and contact curvature govern deformation partitioning between global bending and local contact indentation.
- ii) A proprioceptive finger mechanism that combines a hybrid fingertip with force-transparent quasi-direct drive (QDD) actuators to enable high-fidelity force interaction.
- iii) Experimental validation on contact-rich manipulation, demonstrating that the proposed design substantially amplifies stable pinching and fine manipulation across various objects.

II. RELATED WORK

A. Dexterous Hand Design

Previous robotic hand designs have prioritized achieving sufficient torque output within tight spatial constraints while supporting high-DoF kinematics [29]. Many systems embed high-reduction servo motors directly within the fingers [14, 16, 30], simplifying transmission but adding distal mass and rigidity that reduce compliance and increase vulnerability to impact. The fixed housing geometry of these servo units further constrains finger morphology and limits overall hand form factors.

To mitigate distal mass and geometric constraints, other designs relocate actuators proximally and route motion through tendons [6–11]. While these remote transmissions support more anthropomorphic finger structures, they introduce substantial transmission nonlinearity. Tendon systems suffer from friction, hysteresis, and elastic deformation that degrade force-motion transparency and complicate joint-state estimation, particularly when joints lack encoders. Linkage mechanisms [12, 13, 31] avoid tendon elasticity but often rely on complex closed-chain architectures driven by gear-reduced actuators,

resulting in workspace-dependent transmission ratios and elevated internal forces during contact. Across these approaches, high mechanical impedance or nonlinear transmission behavior remains a barrier to transparent force interaction.

Unlike prior methods, the PLATO Hand employs efficient transmission with QDD actuators and a five-bar mechanism in which only a single joint per finger is routed through the linkage, maintaining low mechanical impedance. This architecture enables transparent contact interaction and reliable proprioceptive force estimation.

B. Compliant Fingertips with Fingernails

Compliant fingertips have been widely explored in robotic fingers to achieve passive adaptation. These range from rubber-like pads attached to rigid fingers to structured flexural fingertips that use distributed compliant elements to conformally wrap around objects [32–35]. However, fully compliant designs face limitations in thin-object acquisition and precise contact initiation, where localized stiffness is beneficial.

Several robotic fingertip designs have incorporated rigid nail structures to achieve this functionality. Early prototypes demonstrated that rigid distal edges increase pinching force and improve thin-object lifting [28, 36]. Recent tactile sensing modules integrate synthetic nails to enable fine edge manipulation with sub-millimeter clearance [25], while multi-finger systems use nails for low-profile object pickup and screw-cap manipulation [24, 26, 37].

Previous robotic fingertip implementations with nails, however, differ substantially from the anatomical fingertip, where the nail is supported by the nail bed and the soft fingerpulp wraps around this internal structure, enabling dorsal support and multi-directional contact. The PLATO Hand adopts an anthropomorphic fingertip architecture that couples a rigid nail, a compliant fingerpulp, and an internal skeletal link, providing the structural basis for the nail to influence contact mechanics and interface effectively with proprioceptive sensing.

III. DESIGN

Here, we present the PLATO Hand, a dexterous robotic hand designed for structured contact mechanics and high-

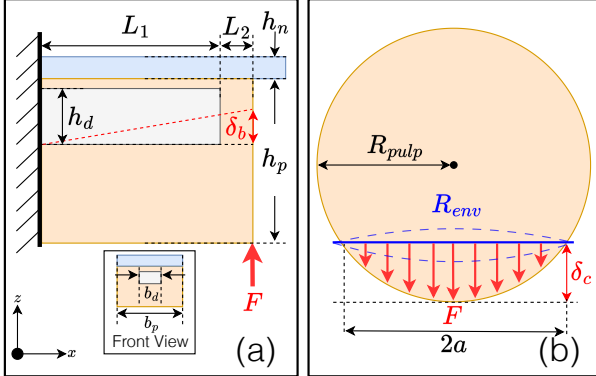


Fig. 3: Strain Energy Fingertip Model. (a) Composite cantilever model of the PLATO Hand fingertip, consisting of a thin, rigid fingernail, soft pulp, and an embedded distal phalanx. The model captures bending deformation through a piecewise flexural rigidity determined by the layered geometry. (b) Hertzian contact model describing local indentation of the pulp against an external surface with radius R_{env} . The indentation depth δ_c determines the contact radius. The total fingertip deformation couples beam bending and contact indentation: $\delta_{total} = \delta_b + \delta_c$.

bandwidth force-regulated interaction. The hand integrates a hybrid fingertip that combines a rigid fingernail with a compliant fingerpulp to shape local contact mechanics. Combined with QDD actuators, a five-bar linkage mechanism provides high force-motion transparency for safe, reactive interaction. The hand comprises three fingers with eight fully actuated DoF, supporting a range of grasping and manipulation tasks.

A. Hybrid Fingertip Design

The PLATO Hand employs a biomimetic fingertip that combines a rigid fingernail with a compliant, deformable fingerpulp to structure local contact mechanics. This hybrid construction separates local contact compliance from global fingertip stiffness, allowing deformation during contact to be shaped independently of overall rigidity.

In this subsection, we analyze how the fingernail–pulp structure governs contact behavior by redistributing deformation away from global bending and toward localized contact indentation. We adopt an energy-based formulation that decomposes fingertip deformation into two components: bending of the fingertip structure and local indentation at the contact interface. Under a prescribed displacement δ_{total} , kinematic compatibility decomposes the deformation into bending and contact indentation, such that $\delta_{total} = \delta_b + \delta_c$. The total elastic energy then separates into

$$U_{total}(\delta_{total}) = U_b(\delta_b) + U_c(\delta_c). \quad (1)$$

The strain energy associated with each deformation mode is obtained from the work–energy principle by integrating the corresponding reaction force over its deformation.

1) *Bending Energy*: We model the fingertip as a bonded layered beam of total length $L = L_1 + L_2$, where the segment spanning $0 \leq x \leq L_1$ includes the distal phalanx, pulp, and fingernail, and the segment $L_1 < x \leq L$ consists of the pulp

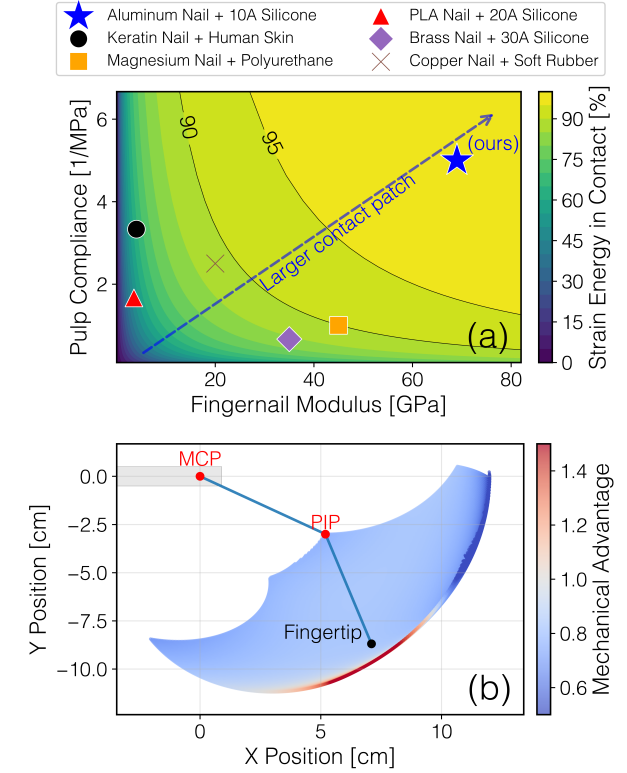


Fig. 4: Energy-based design characterization of the fingertip and finger kinematics. (a) Heatmap of the fraction of strain energy in contact indentation under a fixed fingertip approach. Higher nail stiffness and pulp compliance concentrate deformation at the contact rather than in global bending. The PLATO Hand design achieves over 95% energy concentration in local indentation. (b) Fingertip Cartesian workspace and corresponding mechanical advantage distribution for the optimized linkage, showing reduced variation across the reachable workspace.

and fingernail alone. The resulting flexural rigidity is piecewise constant:

$$EI(x) = \begin{cases} (EI)_1, & 0 \leq x \leq L_1 \quad (\text{distal + pulp + nail}), \\ (EI)_2, & L_1 < x \leq L \quad (\text{pulp + nail}). \end{cases} \quad (2)$$

To obtain a single equivalent stiffness, we define an effective bending rigidity $(EI)_{\text{eff}}$ by equating the strain energy under a tip load to that of a uniform beam.

$$U_b(\delta_b) = \int_0^L \frac{M(x)^2}{2EI(x)} dx = \frac{1}{2} \frac{3(EI)_{\text{eff}}}{L^3} \delta_b^2. \quad (3)$$

2) *Contact Indentation Energy*: We model the fingertip as a sphere contacting a surface under frictionless, non-adhesive, quasistatic loading. The soft pulp is treated as an elastic half-space with effective modulus $E^* = E_p/(1 - \nu_p^2)$, where E_p is the Young's modulus and ν_p is the Poisson ratio of the pulp material. The effective contact radius R_{eff} is determined by the combined curvatures of the fingertip and the environment, and reduces to the fingertip radius R_{pulp} for contact with a flat surface.

Under Hertzian contact, the force-indentation relationship and contact patch radius are given by

$$F(\delta_c) = \frac{4}{3} E^* \sqrt{R_{\text{eff}}} \delta_c^{3/2}, \quad a = \sqrt{R_{\text{eff}} \delta_c}. \quad (4)$$

Applying the work-energy principle, the contact strain energy is

$$U_c(\delta_c) = \int_0^{\delta_c} F d\delta = \frac{8}{15} E^* \sqrt{R_{\text{eff}}} \delta_c^{5/2}. \quad (5)$$

3) *Energy Minimization and Deformation Partitioning*: The internal deformation partition (δ_b, δ_c) is determined by the fingertip structure through energy minimization. For a given externally imposed fingertip approach, the physically realized deformation partition corresponds to the configuration that minimizes the total elastic strain energy.

We model this as a constrained optimization problem:

$$\min_{\delta_b, \delta_c} U_b(\delta_b) + U_c(\delta_c) \quad (6)$$

$$\text{subject to } \delta_b + \delta_c = \delta_{\text{total}}. \quad (7)$$

Solving the first-order optimality conditions yields

$$\delta_c + \beta \delta_c^{3/2} = \delta_{\text{total}}, \quad \beta = \frac{4E^* \sqrt{R_{\text{eff}}} L^3}{9(EI)_{\text{eff}}}. \quad (8)$$

The parameter β governs how deformation is distributed: a rigid fingernail increases $(EI)_{\text{eff}}$, lowers β , and drives deformation into local indentation ($\delta_c \approx \delta_{\text{total}}$), whereas a compliant fingertip raises β and causes bending to dominate.

Substituting the solution for δ_c into the energy expressions gives the total strain energy:

$$U_{\text{total}} = \frac{1}{2} \frac{3(EI)_{\text{eff}}}{L^3} (\delta_{\text{total}} - \delta_c)^2 + \frac{8}{15} E^* \sqrt{R_{\text{eff}}} \delta_c^{5/2}. \quad (9)$$

The contact energy fraction is

$$\eta_{\text{contact}} = \frac{U_c}{U_{\text{total}}} \quad (10)$$

Increasing $(EI)_{\text{eff}}$ through a rigid fingernail drives η_{contact} toward unity and enlarges a_{eff} for a given fingertip approach. This mechanism explains how the fingernail structures local contact mechanics across different object curvatures.

B. Finger Linkage Transmission Design

The finger mechanism employs a five-bar linkage to transmit motion between the actuated joint and the distal joint without collocating actuators at the joints. Due to the linkage kinematics shown in Fig. 2(c), the distal joint motion is nonlinear and depends on the configuration variables ϕ_1 and ϕ_2 . This kinematic nonlinearity results in a configuration-dependent mechanical advantage (MA) between the actuator angle ϕ_2 and the joint angle ϕ_4 [38].

Using loop-closure kinematics and Cramer's rule applied to the mechanism Jacobian, the differential relationship between ϕ_2 and ϕ_4 is

$$N(\phi_2, \phi_4) = \frac{d\phi_2}{d\phi_4} = \frac{-L_4 \sin(\phi_3 - \phi_4)}{L_2 \sin(\phi_2 - \phi_3)}, \quad (11)$$

where $N(\phi_2, \phi_4)$ denotes the geometric mechanical advantage.

Large variations in MA introduce nonlinear distortions in the sensed force-torque relationship, degrading force control accuracy. We therefore optimize the link lengths L_1 and L_3 to reduce MA variation across the configuration space while satisfying geometric and workspace constraints.

The optimization problem is formulated as

$$\min_{L_1, L_3} J = w_1 \|\Delta\theta\|_2 + w_2 \sigma_N + w_3 \text{TI} + w_4 \|\mathbf{L}\|_2^2 \quad (12a)$$

$$\text{s.t. } \sum_{i=1}^5 L_i e^{j\phi_i} = 0 \quad (12b)$$

$$\mathbf{L}_{\min} \leq \mathbf{L} \leq \mathbf{L}_{\max}, \quad (12c)$$

where the objective terms are defined as follows:

- $\|\Delta\theta\|_2$: workspace coverage.
- σ_N : mechanical advantage variation.
- TI : transmission index.
- $\|\mathbf{L}\|_2^2$: link length regularization.

The constraints enforce geometric closure of the linkage and restrict link lengths to physically feasible ranges.

The resulting nonlinear optimization problem is solved using the Covariance Matrix Adaptation Evolution Strategy (CMA-ES), which is suitable for non-convex design spaces with multiple local minima [39]. The resulting workspace and MA distribution are shown in Fig. 4(b).

C. Hand Topology Design

The PLATO Hand is formed by assembling three instances of the finger design described above, each actuated by 1:8 QDD actuators [40]. The thumb includes two additional proximal degrees of freedom actuated by compact servo motors [41], while the remaining joints are driven by the finger mechanisms. This topology supports a range of common three-finger grasping configurations [42].

IV. EXPERIMENTS

We examine how the mechanical design of the PLATO Hand shapes contact interaction. Using the PLATO Hand mounted on a 7-DoF robotic manipulator [43], we evaluate three aspects: (1) pinching stability across object geometries, (2) contact force observability through texture sensing and proprioceptive feedback, and (3) performance in contact-rich manipulation tasks involving thin or delicate objects. Together, these experiments demonstrate how interaction behaviors emerging from fingertip mechanics support effective manipulation.

A. Pull-Out Experiments on Hybrid Fingertip Mechanics

To evaluate pinching stability under tangential disturbance, we performed pull-out experiments on planar, concave, and convex objects using 10A and 20A silicone pulps, with and without a fingernail. We applied an identical normal preload in all conditions and translated the object upward until failure, recording the maximum pull-out force (Fig. 5(a)).

Across all geometries, the presence of the fingernail consistently increased maximum pull-out force. On planar surfaces, both 10A and 20A pulps benefited from the fingernail, with the softer material exhibiting slightly higher stability due to increased conformity. On concave and convex surfaces, the influence of the fingernail became more pronounced. Without the fingernail, the softer 10A pulp exhibited reduced stability on

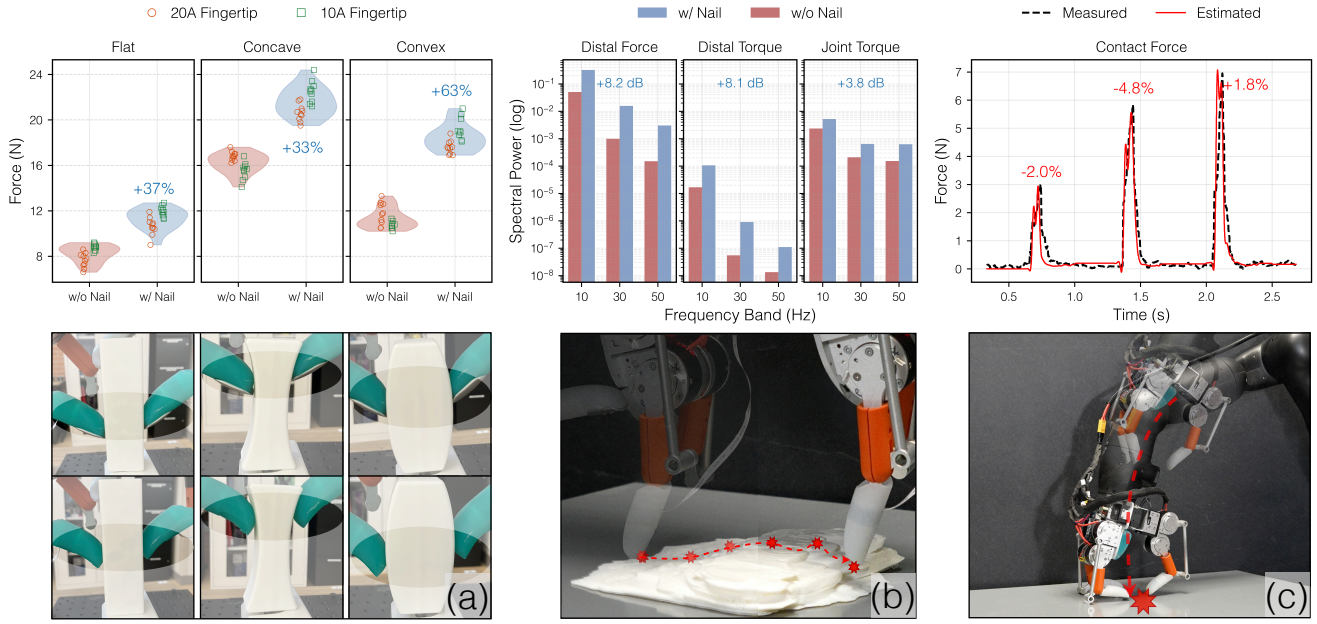


Fig. 5: Experimental evaluation of the PLATO Hand. (a) Pinching stability evaluated through pullout experiments on flat, concave, and convex geometries, comparing hybrid fingertips with a rigid fingernail (top) and pulp-only fingertips without a fingernail (bottom). The fingernail consistently increases pullout force across all geometries, with enhanced effectiveness on curved surfaces where it constrains local deformation and preserves contact area. (b) Texture sensing experiment comparing the frequency-domain responses of the hybrid and pulp-only fingertips. The bar plots show integrated spectral power computed over three frequency ranges (0–10 Hz, 10–30 Hz, and 30–50 Hz). Across all bands, the hybrid fingertip exhibits higher spectral energy, indicating enhanced sensitivity to contact-induced texture variations enabled by the fingernail. (c) High-speed impact experiment demonstrating proprioceptive force estimation during dynamic contact. Estimated contact forces using Kalman filtering closely track distal force-torque sensor measurements along the finger flexion-extension axis across three impact events, with tracking error remaining below 5%.

curved geometries, as excessive deformation limited effective contact. In contrast, the presence of the fingernail suppressed this degradation, allowing the softer pulp to maintain stable contact even under curvature.

This curvature-dependent trend is consistent with the deformation partitioning described by our coupled bending-indentation model (8). When object curvature is present, contact stability becomes increasingly sensitive to the deformation partitioning parameter β . Softer fingertips without a fingernail exhibit a higher β , leading to a reduced indentation depth δ_c and degraded tangential stability on curved surfaces. Since the contact patch scales as $a \propto \sqrt{R_{\text{eff}}\delta_c}$, preserving δ_c is essential for maintaining effective contact. The fingernail lowers β and preserves local indentation, explaining why its stabilizing effect becomes more pronounced in the presence of object curvature.

B. Force Sensing Characterization

We evaluate how the hybrid fingertip influences force sensing during contact, focusing on signal transmission through both distal sensing and proprioceptive estimation.

1) *Contact Force Sensitivity*: To characterize contact sensitivity, we recorded force-torque measurements and motor torque estimates while the index finger traced a textured surface under impedance control. Spectral power was compared across three frequency bands for configurations with and without the fingernail.

As shown in Fig. 5(b), the hybrid fingertip exhibits consistently higher spectral energy, with approximately 8 dB increase

TABLE I: Manipulation Tasks Success Rates

Task	Without Fingernail	With Fingernail
Paper singulation	0/10	8/10
Lid opening	4/10	9/10
Orange peeling	0/3	3/3
Coin picking	0/10	9/10
Card picking	0/10	10/10
Card flipping	0/10	8/10

around 10 Hz and over 20 dB above 30 Hz. This indicates that the rigid fingernail more effectively transmits high-frequency contact variations, while the soft-only fingertip attenuates these components due to material damping.

2) *High-Bandwidth Proprioceptive Force Estimation*: To evaluate proprioceptive sensing during dynamic contact, we performed high-speed impact tests by manually driving the manipulator into a rigid surface. Proprioceptive force estimates were compared against distal force-torque measurements.

As shown in Fig. 5(c), the proprioceptive estimates closely track the distal measurements across impact events, with errors below 5%. This result indicates that the low mechanical impedance of the finger mechanism enables reliable force estimation even during rapid contact transitions.

C. Manipulation Task Demonstrations

We evaluate the PLATO Hand on manipulation tasks that require structured contact geometry and force-aware interaction. All experiments use task-space control of the robotic arm and a predefined grasp state machine with compliant, force-aware

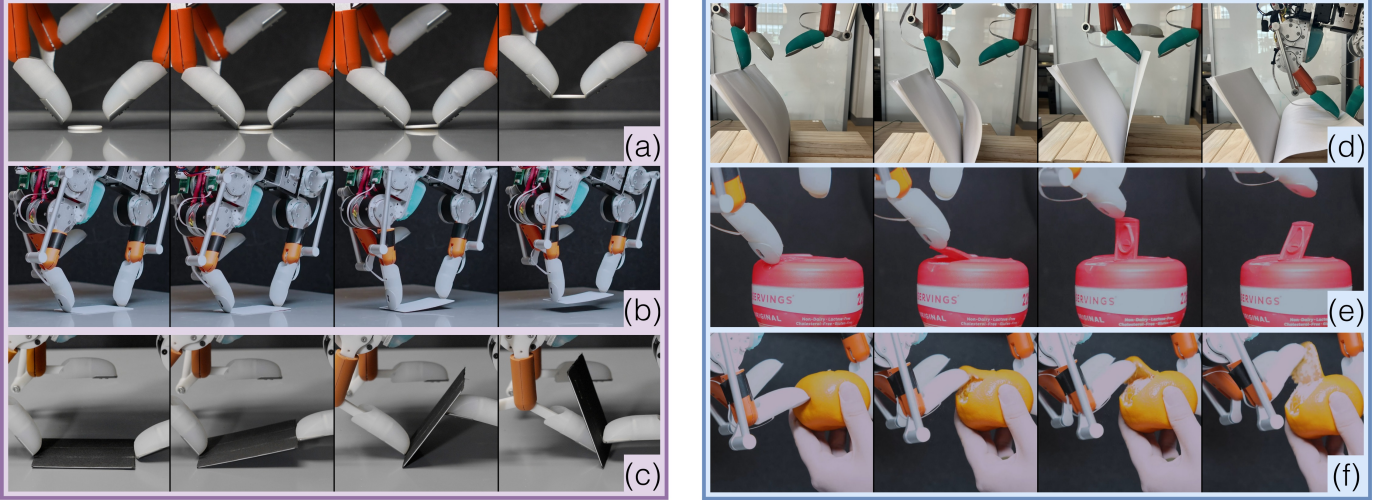


Fig. 6: Teleoperated manipulation tasks demonstrating the PLATO Hand’s dexterity. (a) Coin picking and (b) card picking — retrieving thin objects from a flat surface; (c) card flipping — initiating rotation and grasping a card; (d) paper singulation — isolating and pulling a single sheet from a stack; (e) lid opening — prying open a sealed container; (f) orange peeling — puncturing and following the peel along a curved fruit surface. These tasks highlight how hybrid contact and proprioceptive actuation together enable delicate, contact-rich manipulation without complex motion planning.

behaviors. Table I reports success rates with and without the fingernail.

1) *Rigid Edge Interaction Tasks*: These tasks require the fingertip to form a rigid edge and transmit localized forces through a small contact area.

- **Paper singulation**: Wedge interaction with sub-millimeter gaps between stacked A4 papers.
- **Lid opening**: Edge contact and torque transmission at a predefined leverage point.
- **Orange peeling**: Concentrated force application to puncture and tear the surface.

Without the fingernail, all tasks fail because the compliant pulp deforms before edge contact is established. With the fingernail, the required contact geometry is maintained, leading to substantially higher success rates. Remaining failures are due to poor initial alignment rather than limitations of the fingertip mechanics.

2) *Contact-Rich Manipulation Tasks*: These tasks involve frequent contact transitions under low-force interaction and require precise contact geometry together with compliant force regulation.

- **Coin picking**: Lift initiation on a rigid, low-profile object.
- **Card picking**: Edge interaction and stabilization of a thin, flexible object.
- **Card flipping**: Torque application at an object edge during controlled rotation.

Without the fingernail, all tasks fail due to pulp deformation during contact initiation. With the fingernail, stable contact geometry enables successful task execution. Remaining failures arise from initial misalignment and are exacerbated by repeated contact transitions. These results show that manipulation capability in the PLATO Hand emerges from the integration of mechanically structured contact and proprioceptive, force-regulated actuation.

V. CONCLUSION

In this work, we introduced the PLATO Hand, a proprioceptive robotic hand with a mechanically structured hybrid fingertip designed to shape contact deformation for reliable contact-rich manipulation. By integrating a rigid nail into a compliant, skin-like fingertip, the design reshapes contact deformation in ways that conventional fingertips based on rigid beams with soft traction pads cannot. As a result, the hand enables fine manipulation capabilities such as edge-based interaction on thin and curved objects and supports stable grasping across a range of postures, including lateral pinch.

To extend this architecture to higher-DoF systems, several design constraints must be addressed. Space constraints require smaller motors, which demand higher gear ratios to achieve sufficient torque density. Although well-optimized transmissions preserve the linear current-torque relationship for proprioceptive actuation in quasi-static regimes, reflected inertia inevitably increases. How reflected inertia affects dexterous manipulation performance is task-dependent and remains an open design question. Moreover, extended transmission mechanisms introduce nonidealities such as friction and hysteresis that degrade force-motion transparency. Future work will address these challenges through systematic design optimization to balance gear ratio, reflected inertia, transmission complexity, and task-specific manipulation performance in scalable dexterous hands.

ACKNOWLEDGEMENT

This work was supported by Sony Group Corporation.

REFERENCES

[1] S. C. Jacobsen, E. K. Iversen, D. F. Knutti, R. T. Johnson, and K. B. Biggers, "Design of the utah/M.I.T. dexterous hand," in *Proceedings of the 1986 IEEE International Conference on Robotics and Automation (ICRA)*, vol. 3, 1986, pp. 1520–1532.

[2] C. S. Lovchik and M. A. Diftler, "Robonaut hand: A dexterous robot hand for space," in *Proceedings of the 1999 IEEE International Conference on Robotics and Automation (ICRA)*, vol. 2, 1999, pp. 907–912.

[3] H. Kawasaki, T. Komatsu, and K. Uchiyama, "Dexterous anthropomorphic robot hand with distributed tactile sensor: Gifu hand II," *IEEE/ASME Transactions on Mechatronics*, vol. 7, no. 3, pp. 296–303, 2002.

[4] H. Liu et al., "Multisensory five-finger dexterous hand: The DLR/HIT hand II," in *2008 IEEE/RSJ International Conference on Intelligent Robots and Systems (IROS)*, 2008, pp. 3692–3697.

[5] A. D. Deshpande et al., "Mechanisms of the anatomically correct testbed hand," *IEEE/ASME Transactions on Mechatronics*, vol. 18, no. 1, pp. 238–250, 2013.

[6] Y.-J. Kim, J. Yoon, and Y.-W. Sim, "Fluid lubricated dexterous finger mechanism for human-like impact absorbing capability," *IEEE Robotics and Automation Letters*, vol. 4, no. 4, pp. 3971–3978, 2019.

[7] Y. Toshimitsu et al., "Getting the ball rolling: Learning a dexterous policy for a biomimetic tendon-driven hand with rolling contact joints," in *2023 IEEE-RAS International Conference on Humanoid Robots (Humanoids)*, 2023, pp. 1–7.

[8] C. C. Christoph et al., "ORCA: An open-source, reliable, cost-effective, anthropomorphic robotic hand for uninterrupted dexterous task learning," 2025. arXiv: 2504.04259 [cs.RO].

[9] S. Yang et al., "TRX-Hand5: An anthropomorphic hand with integrated tactile feedback for grasping and manipulation in human environments," in *2024 IEEE/RSJ International Conference on Intelligent Robots and Systems (IROS)*, 2024, pp. 5289–5296.

[10] C. D. Santina, C. Piazza, G. Grioli, M. G. Catalano, and A. Bicchi, "Toward dexterous manipulation with augmented adaptive synergies: The pisa/IIT softhand 2," *IEEE Transactions on Robotics*, vol. 34, no. 5, pp. 1141–1156, 2018.

[11] *Shadow dexterous hand series – research and development tool*, <https://shadowrobot.com/dexterous-hand-series/>.

[12] U. Kim et al., "Integrated linkage-driven dexterous anthropomorphic robotic hand," *Nature Communications*, vol. 12, no. 1, 2021.

[13] G. Li, X. Liang, Y. Gao, T. Su, Z. Liu, and Z.-G. Hou, "A linkage-driven underactuated robotic hand for adaptive grasping and in-hand manipulation," *IEEE Transactions on Automation Science and Engineering*, vol. 21, no. 3, pp. 3039–3051, 2024.

[14] R. Bhirangi et al., "All the feels: A dexterous hand with large-area tactile sensing," *IEEE Robotics and Automation Letters*, vol. 8, no. 12, pp. 8311–8318, 2023.

[15] Wonik Robotics, *Allegro hand*, <https://www.allegrohand.com/>.

[16] *DG-5F | humanoid robotic hand for dexterous manipulation*, <https://en.tesollo.com/dg-5f/>.

[17] P. M. Wensing, A. Wang, S. Seok, D. Otten, J. Lang, and S. Kim, "Proprioceptive actuator design in the MIT cheetah: Impact mitigation and high-bandwidth physical interaction for dynamic legged robots," *IEEE Transactions on Robotics*, vol. 33, no. 3, pp. 509–522, 2017.

[18] Y. Sim and J. Ramos, "The dynamic effect of mechanical losses of transmissions on the equation of motion of legged robots," in *Proceedings of the IEEE International Conference on Robotics and Automation (ICRA)*, 2021, pp. 1191–1197.

[19] G.-C. Jeong, A. Bahety, G. Pedraza, A. D. Deshpande, and R. Martín-Martín, "BaRiFlex: A robotic gripper with versatility and collision robustness for robot learning," in *2024 IEEE/RSJ International Conference on Intelligent Robots and Systems (IROS)*, 2024, pp. 4106–4113.

[20] A. M. Okamura, N. Smaby, and M. R. Cutkosky, "An overview of dexterous manipulation," in *Proceedings 2000 ICRA. Millennium Conference. IEEE International Conference on Robotics and Automation. Symposia Proceedings*, vol. 1, 2000, pp. 255–262.

[21] I. M. Bullock, R. R. Ma, and A. M. Dollar, "A hand-centric classification of human and robot dexterous manipulation," *IEEE Transactions on Haptics*, vol. 6, no. 2, pp. 129–144, 2013.

[22] B. M. Piraccini, "Nail anatomy and physiology for the clinician," in *Nail Disorders*, Springer, 2014, pp. 1–6.

[23] R. Shirato, A. Abe, H. Tsuchiya, and M. Honda, "Effect of fingernail length on the hand dexterity," *Journal of Physical Therapy Science*, vol. 29, no. 11, pp. 1914–1919, 2017.

[24] H.-S. Fang et al., *DEXOP: A device for robotic transfer of dexterous human manipulation*, 2025. arXiv: 2509.04441 [cs.RO].

[25] W. K. Do, A. K. Dhawan, M. Kitzmann, and M. Kennedy, "DenseTact-Mini: An optical tactile sensor for grasping multi-scale objects from flat surfaces," in *Proceedings of the IEEE International Conference on Robotics and Automation (ICRA)*, 2024, pp. 6928–6934.

[26] S. Jain, T. Stalin, V. Subramaniam, J. Agarwal, and P. V. Y. Alvarado, "A soft gripper with retractable nails for advanced grasping and manipulation," in *2020 IEEE International Conference on Robotics and Automation (ICRA)*, 2020, pp. 6928–6934.

[27] L. Odhner et al., "A compliant, underactuated hand for robust manipulation," *The International Journal of Robotics Research*, vol. 33, pp. 736–752, 2013.

[28] K. Murakami and T. Hasegawa, "Novel fingertip equipped with soft skin and hard nail for dexterous multi-fingered robotic manipulation," in *Proceedings of the IEEE International Conference on Robotics and Automation (ICRA)*, vol. 1, 2003, pp. 708–713.

[29] C. Piazza, G. Grioli, M. G. Catalano, and A. Bicchi, "A century of robotic hands," *Annual Review of Control, Robotics, and Autonomous Systems*, vol. 22, pp. 1–32, 2019.

[30] K. Shaw, A. Agarwal, and D. Pathak, "LEAP hand: Low-cost, efficient, and anthropomorphic hand for robot learning," in *Robotics: Science and Systems (RSS)*, 2023.

[31] S. R. Kashef, S. Amini, and A. Akbarzadeh, "Robotic hand: A review on linkage-driven finger mechanisms of prosthetic hands and evaluation of the performance criteria," *Mechanism and Machine Theory*, vol. 145, p. 103677, 2020.

[32] W. Crooks, G. Vukasin, M. O'Sullivan, W. Messner, and C. Rogers, "Fin Ray® effect inspired soft robotic gripper: From the RoboSoft grand challenge toward optimization," *Frontiers in Robotics and AI*, vol. 3, p. 220991, 2016.

[33] C. Chi et al., "Universal manipulation interface: In-the-wild robot teaching without in-the-wild robots," in *Proceedings of Robotics: Science and Systems (RSS)*, 2024.

[34] M. Seo, H. A. Park, S. Yuan, Y. Zhu, and L. Sentis, "LEGATO: Cross-embodiment imitation using a grasping tool," *IEEE Robotics and Automation Letters*, pp. 1–8, 2025.

[35] S. Shang, M. Seo, Y. Zhu, and L. Chin, *FORTE: Tactile force and slip sensing on compliant fingers for delicate manipulation*, 2025. arXiv: 2506.18960 [cs.RO].

[36] A. Kumagai, Y. Obata, Y. Yabuki, Y. Jiang, H. Yokoi, and S. Togo, "Comparison of precision grasping performance between artificial fingers with and without nails," in *2022 IEEE 4th Global Conference on Life Sciences and Technologies (LifeTech)*, 2022, pp. 380–381.

[37] J. S. Torrey, J. F. Morrow, R. D. Larkins, and S. T. Dang, "Improving soft pneumatic actuator fingers through integration of soft sensors, position and force control, and rigid fingernails," *Tech. Rep.*, 2015.

[38] B. Zi, J. Cao, and Z. Zhu, "Dynamic simulation of hybrid-driven planar five-bar parallel mechanism based on SimMechanics and tracking control," *International Journal of Advanced Robotic Systems*, vol. 8, no. 4, pp. 28–33, 2011.

[39] N. Hansen, *The CMA evolution strategy: A tutorial*, 2023. arXiv: 1604.00772 [cs.LG].

[40] *SteadyWin GIM3505-8*, <https://steadywin.cn/en/pd.jsp?id=130>.

[41] *ROBOTIS XM430-W350-T/R*, <https://emanual.robottis.com/docs/en/dxl/xm430-w350/>.

[42] M. R. Cutkosky, "On grasp choice, grasp models, and the design of hands for manufacturing tasks," *IEEE Transactions on Robotics and Automation*, vol. 5, no. 3, pp. 269–279, 1989.

[43] *Roboligent | intelligent manufacturing automation*, Roboligent, 2025.

APPENDIX

A. PLATO Hand Specifications

TABLE II: Optimized linkage dimensions and PLATO Hand specifications.

Parameter	Value
Optimized linkage dimensions	
L_1	30.0 mm
L_2	100.25 mm
L_3	20.5 mm
L_4	60.0 mm
L_5	40.4 mm
PLATO Hand specifications	
Total mass	1.3 kg
Degrees of freedom	8
Extended finger length	120 mm
Maximum payload	11.3 kg
Fingertip force	5–15 N
Rated power	30 W
Communication	CAN (1 kHz)

B. Composite Beam Flexural Rigidity

The cross-section consists of the pulp (p), nail (n), and distal phalanx (d). For the proximal segment ($0 \leq x \leq L_1$), the geometric properties are:

$$\begin{aligned} A_p &= b_p h_p - b_d h_d, & y_{gross} &= h_p/2, \\ A_d &= b_d h_d, & y_{void} &= h_p - h_d/2, \\ A_n &= b_p h_n, & y_n &= h_p + h_n/2. \end{aligned}$$

The neutral axis is $\bar{y}_1 = \frac{E_p A_p y_p + E_d A_d y_{void} + E_n A_n y_n}{E_p A_p + E_d A_d + E_n A_n}$.

The second moments of area are calculated below. Crucially, I_p^c applies the parallel axis theorem to subtract the eccentric void (distal phalanx) from the pulp:

$$\begin{aligned} I_d^c &= \frac{1}{12} b_d h_d^3, & I_n^c &= \frac{1}{12} b_p h_n^3, \\ I_p^c &= \left[\frac{b_p h_p^3}{12} + b_p h_p (y_{gross} - y_p)^2 \right] \\ &\quad - \left[\frac{b_d h_d^3}{12} + b_d h_d (y_{void} - y_p)^2 \right]. \end{aligned}$$

The total flexural rigidity is the sum of stiffness contributions:

$$(EI)_1 = \sum_{k \in \{p, d, n\}} E_k [I_k^c + A_k (y_k - \bar{y}_1)^2].$$

For the distal segment ($L_1 < x \leq L$), the distal phalanx is absent. The properties $A_p^{(2)}, A_n^{(2)}$ and $(EI)_2$ are calculated similarly with $E_d = 0$.

C. Effective Rigidity from Energy Equivalence

For a tip force F at $x = L$, the bending moment is $M(x) = F(L - x)$. The strain energy of the piecewise beam is

$$U_b^{\text{comp}} = \frac{1}{2} \left[\int_0^{L_1} \frac{M(x)^2}{(EI)_1} dx + \int_{L_1}^L \frac{M(x)^2}{(EI)_2} dx \right].$$

Substituting $L_2 = L - L_1$ and evaluating the integrals:

$$\int_0^{L_1} (L - x)^2 dx = \frac{L^3 - L_1^3}{3}, \quad \int_{L_1}^L (L - x)^2 dx = \frac{L_2^3}{3}.$$

This yields:

$$U_b^{\text{comp}} = \frac{F^2}{6} \left[\frac{L^3 - L_1^3}{(EI)_1} + \frac{L_2^3}{(EI)_2} \right].$$

A uniform beam of rigidity $(EI)_{\text{eff}}$ has energy $U_b^{\text{eff}} = F^2 L^3 / [6(EI)_{\text{eff}}]$. Equating energies and solving:

$$(EI)_{\text{eff}} = \frac{L^3}{\frac{L^3 - L_1^3}{(EI)_1} + \frac{L_2^3}{(EI)_2}}.$$

For a uniform cantilever under tip load F , the tip deflection is $\delta_b = FL^3 / [3(EI)_{\text{eff}}]$. Inverting and substituting into the energy expression:

$$U_b(\delta_b) = \frac{1}{2} \frac{3(EI)_{\text{eff}}}{L^3} \delta_b^2.$$

D. Hertzian Contact Indentation

Based on Hertzian contact theory with effective pulp modulus $E^* = E_p / (1 - \nu_p^2)$ and effective radius R_{eff} , the force-indentation relationship is

$$F(\delta_c) = \frac{4}{3} E^* \sqrt{R_{\text{eff}}} \delta_c^{3/2}.$$

Integrating the work done during indentation:

$$U_c(\delta_c) = \int_0^{\delta_c} F(\delta) d\delta = \frac{8}{15} E^* \sqrt{R_{\text{eff}}} \delta_c^{5/2}.$$

E. Lagrangian Formulation for Energy Minimization

The partitioning of deformation minimizes total elastic energy subject to $\delta_{\text{total}} = \delta_b + \delta_c$. The Lagrangian is

$$\mathcal{L}(\delta_b, \delta_c, \lambda) = U_b(\delta_b) + U_c(\delta_c) + \lambda(\delta_{\text{total}} - \delta_b - \delta_c).$$

First-order optimality conditions:

$$\frac{\partial \mathcal{L}}{\partial \delta_b} = \frac{3(EI)_{\text{eff}}}{L^3} \delta_b - \lambda = 0,$$

$$\frac{\partial \mathcal{L}}{\partial \delta_c} = \frac{4}{3} E^* \sqrt{R_{\text{eff}}} \delta_c^{3/2} - \lambda = 0.$$

Eliminating λ and using $\delta_b = \delta_{\text{total}} - \delta_c$ yields

$$\delta_c + \beta \delta_c^{3/2} = \delta_{\text{total}}, \quad \beta = \frac{4E^* \sqrt{R_{\text{eff}}} L^3}{9(EI)_{\text{eff}}}.$$